Hindawi
Journal of Nanomaterials
Volume 2019, Article ID 8628354, 10 pages
https://doi.org/10.1155/2019/8628354

Research Article

The One-Step Preparation of Green-Emissioned Carbon Dots through Hydrothermal Route and Its Application

Jun Li,[1,2] Shiyao Ma,[1,2] Xincai Xiao,[1,2] and Dan Zhao[1,2]

[1]*School of Pharmaceutical Sciences, South-Central University for Nationalities, Wuhan 430074, China*
[2]*National Demonstration Center for Experimental Ethnopharmacology Education (South-Central University for Nationalities), Wuhan 430074, China*

Correspondence should be addressed to Dan Zhao; wqzhdpai@163.com

Received 3 October 2018; Revised 28 November 2018; Accepted 21 February 2019; Published 17 April 2019

Academic Editor: Marinella Striccoli

This paper reports the preparation of green-emissioned CDs by a one-step hydrothermal route with DL-malic acid and ethylenediamine as raw materials and further explored the impacts of the amount of reactants, the reaction time, and temperature upon the optical properties of prepared CDs, to select the optimal preparation parameters. The optical properties, surface groups, and element components of the prepared CDs have been systematically studied by UV-Vis absorption spectra, fluorescence spectra, FTIR, EDS, and XPS. The prepared CDs have been applied to realize the fingerprint development, fluorescence ink, and, specifically, the detection of Fe^{2+} through an inner filter effect with its detection range at $2.0 \times 10^{-7} - 2.3 \times 10^{-5}$ mol/L.

1. Introduction

In recent years, carbon dots (CDs), as a novel fluorescent carbon nanomaterial, have been widely applied in the fields of biological sensor [1, 2], biological imaging [3, 4], drug delivery [5, 6], photocatalysis [7], and light-emitting diodes [8], thanks to their unique properties, such as excellent biological compatibility, stable photoluminescence, and easy surface functionalization [1]. However, most blue-emissioned CDs can cause damage to cells and organisms [9]. Therefore, the preparation of long-wavelength CDs is essential for the better application of CDs in the fields of sensor and biological imaging.

Thus, researchers have developed more CDs with long-wavelength emission, including green- [10–13], yellow- [14–16], and red-emissioned [17–23] CDs. Gu et al. have prepared green-emissioned CDs through a microwave route with crane sugar as carbon source and diethylene glycol (DEG) as reaction media [24]. Dong and his group acquired orange-emissioned CDs through a microwave route with *p*-phenylenediamine as raw material and ethambutol as solvent [14]. Xu et al. used selenocystine as a raw material and have acquired Se-doped green-emissioned CDs with QYs at 7.6% through the hydrothermal route (60°C, 24 h) [25]. The adjustment of the emission wavelength of prepared CDs is mostly through the selection of raw materials, without noticing the impacts of other synthesis parameters upon the optical properties of prepared CDs. Some research teams have reported the adjustment of reaction solvents; reaction temperature and time could effectively change the emission wavelength of prepared CDs. Ding et al. have acquired PL emission from blue to NIR CDs with o-phenylenediamine and L-glutamic acid as raw materials, and formamide, dimethylformamide (DMF), ethanol, and H_2SO_4 aqueous solution as solvents [26]. Chen and his team used *p*-phenylenediamine as carbon source and acquired orange-emissioned CDs (200°C, 1 h) and blue-emissioned ones (160°C, 6 h) [27]. Therefore, the systematic investigation of synthesis parameters is essential for adjustment of CD emission and further understanding of their emission mechanism.

Some reported CDs have already exhibited excellent optical stability, pH stability, salt stability, and ability against the interference of metal ions and thus have been widely applied in the fields of fingerprint development and imaging [28],

fluorescence ink [29], and LED [30]. However, the application of these CDs as fluorescence sensor for metal detection are mostly based on photoinduced electron transfer (PET) [31, 32], which is not sensitive enough to realize specific and selective detection to target metal ions. New detection models are thus essential. Recently, a new fluorescence sensor based on inner filter effect (IFE) has attracted the interest of the researchers [33, 34]. IFE quenches the fluorescence of fluorophores through the absorption of excitation light and/or emission light by the absorber, without any requirements of coupling or electrostatic binding between the detection objects and the fluorescent probe, endowing better selectivity and suitability for analysis applications. However, the low concentration of metal ions in the aqueous phase could hardly change the fluorescence of CDs through IFE. The proper developer would interact with the metal ions to form a colored complex with strong absorption ability, leading to a dramatic change in CD fluorescence. This method exhibits excellent selectivity and sensitivity.

Iron is one of the most important elements for the biological system, with its involvement in many physiological processes, such as oxygen delivery [35], enzymatic reactions [36], and electron transfer in the mitochondrial respiratory chain [37]. But the excessive accumulation of iron in the human body would lead to various diseases, including hepatitis [38], Alzheimer's disease [39], and Parkinson's disease [40]. Iron exists in two forms of compound forms: reductive Fe^{2+} and oxidizing Fe^{3+}. These two forms exhibit a dramatic difference in physiological activity. The present detections mainly focus on Fe^{3+} and Fe ions [41–43], so the development of a fast and accurate detection method to Fe^{2+} is of crucial importance.

This paper reports the preparation of green-emissioned CDs through a hydrothermal route with DL-malic acid and EDA as raw materials and explores the impacts of the ratio of reactants, reaction time, and temperature upon the fluorescence intensity of CDs to get the optimal reaction parameters. The optical properties, surface groups, and element components of the prepared CDs have been systematically studied by UV-Vis absorption spectra, fluorescence spectra, FTIR, EDS, and XPS. The CDs exhibit excellent stability and have been successfully applied in fingerprint development, fluorescence ink, and specifically detection of Fe^{2+} through the inner filter effect.

2. Experimental

2.1. Materials. DL-Malic acid, polyacrylic acid (PAA), cadmium chloride ($CdCl_2$), rhodamine 6G, and silver nitrate were ($AgNO_3$) obtained from Aladdin Chemistry Co. Ltd. Ethylenediamine (EDA), manganese(II) chloride tetrahydrate ($MnCl_2$), cobalt(II) chloride hexahydrate ($CoCl_2$), zinc chloride ($ZnCl_2$), iron(II) sulfate heptahydrate ($FeSO_4$), iron(III) chloride hexahydrate ($FeCl_3$), 1,10-phenanthroline (o-phen), acetic acid (HAc), urea, glycerol (GI), citric acid (CA), ethylenediaminetetraacetic acid disodium salt (EDTA-2Na), lead(II) acetate trihydrate ($(CH_3COO)_2Pb$), copper(II) chloride dehydrate ($CuCl_2$), and calcium chloride anhydrous ($CaCl_2$) were obtained from Sinopharm Chemical Reagent Co. Ltd. Mercuric chloride ($HgCl_2$) was obtained from Tongren Chemical Reagent Factory. Ferrous sulfate syrup was obtained from Inner Mongolia Hefu Pharmaceuticals Co. Ltd. (serial number: 03180401 015).

2.2. Instrumentation. The DHG-9030-type electric thermostatic blast drying oven (Shanghai Yiheng Technology Company) was used to synthesize CDs, and UV-Vis absorption spectra were recorded on a Lambda-35 UV/Vis spectrophotometer (PerkinElmer Company). Fluorescence spectra were acquired with a LS55 spectrofluorometer (PerkinElmer Company). Fourier transform infrared spectra were obtained on a Nicolet 6700 (FTIR) spectrometer (Thermo Fisher Scientific). EDS patterns were captured using an FEI Quanta 200 scanning electron microscope equipped with an energy-dispersive X-ray spectrometer (FEI Company). XPS measurements were acquired with a VG MultiLab 2000 X-ray photoelectron spectrometer (Thermo Electron Corporation). Structural investigations were carried out by X-ray diffractometry (XRD, Bruker D8 Advance, Germany).

2.3. Preparation of the CDs. In a typical preparation procedure, 1.0 g DL-malic acid and 0.4 mL EDA were mixed in 20 mL of water under stirring, followed by deaerating with high-purity nitrogen gas for 20 min. Finally, the solution was transferred into a 25 mL Teflon-lined autoclave. It was loaded in an oven at 200°C for 4 h and then cooled to room temperature naturally. The QY of CDs was measured according to the literature [44]. Rhodamine 6G in ethanol was chosen as the reference standard (QY = 95%). The PL intensity was measured by an LS55 spectrofluorometer with λ_{ex} = 460 nm. The measured wavelength range was 470-700 nm. Excitation and emission slits were 10 nm and 6 nm, respectively. During fluorescence measurement, the concentration of CDs was 1/10 of the original concentration, unless otherwise specified.

The purification of CDs was as follows. Acetonitrile was added to the CD solution (volume ratio of CDs to acetonitrile was 1: 3). The solution was then centrifuged at 5000 r/min for 5 min. The precipitate after centrifugation was freeze-dried to a solid and stored for future use.

3. Results and Discussion

3.1. Synthesis and Characterization of CDs

3.1.1. The Impact of EDA Amount upon Prepared CDs. CDs have been prepared through a hydrothermal route with DL-malic acid and EDA. The impacts of the amount of reactants, reaction time, and temperature upon the optical properties of prepared CDs have been investigated. With other reaction parameters fixed (1.0 g DL-malic acid, 200°C, 4 h), the amount of EDA was optimized. As shown in Figure 1(a), the fluorescence intensity increases with the increased amount of EDA and reaches the maximum when the EDA amount is at 0.4 mL. Further increase of EDA would cause fluorescence decrease. Moreover, the emission peak of prepared CDs red-shifts from 498 nm to 528 nm with the increased EDA amount. EDA works both as the doping agent

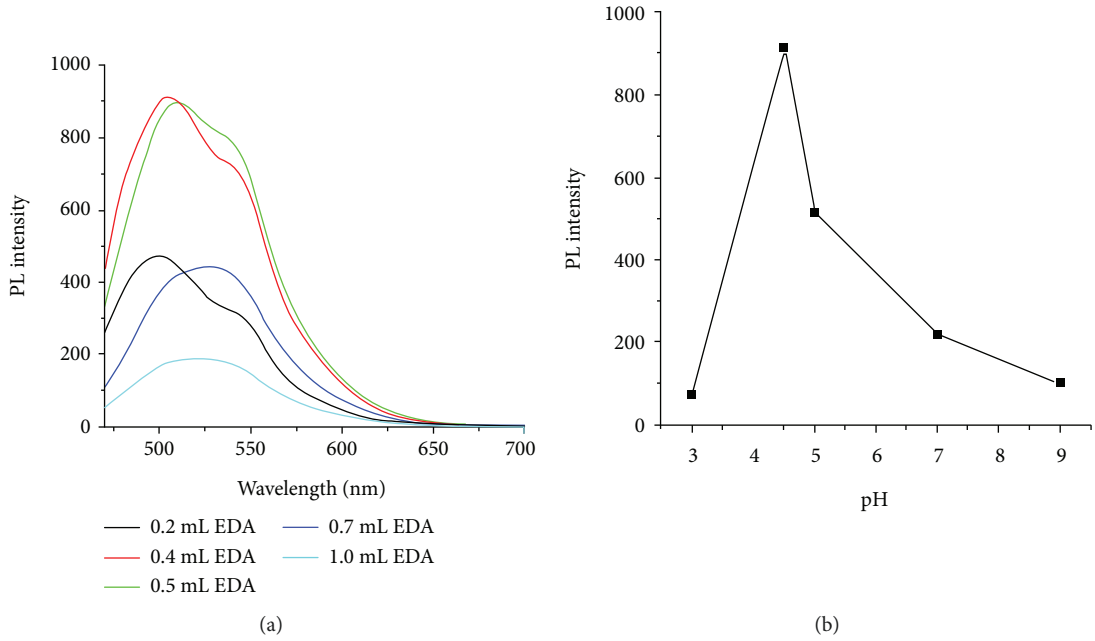

Figure 1: Effect of EDA amount (a) and pH value (b) of CDs (λ_{ex} = 460 nm).

of N element and as the surface passivation agent [45]. According to the previous reports, the doping of the N element could effectively enhance the fluorescence intensity of prepared CDs [46], and the existence of the passivation agent could decrease the surface defects of CDs [47]. Therefore, the enhanced amount of EDA could lead to improved fluorescence intensity, while, on the other hand, because EDA is strongly alkaline, the excessive amount of EDA would enhance the pH value of the precursor solution, which is not conducive to the synthesis of CDs. Therefore, the optimal EDA amount is 0.4 mL.

With other experimental factors fixed, the pH value of the precursor solution was investigated. As illustrated in Figure 1(b), the pH value greatly impacts the PL intensity of prepared CDs. The PL intensity gradually enhances with the increase in pH from 3 to 4.5. However, when the pH value increases from 4.5 to 9, the PL intensity of the CDs obviously decreases. The optimal pH value is thus set at 4.5.

3.1.2. The Impacts of Reaction Temperature and Time upon CDs. With other reaction parameters fixed (1.0 g DL-malic acid and 0.4 mL EDA, 4 h), the impact of reaction temperature upon the optical properties of prepared CDs was explored. As shown in Figure 2(a), the optimal reaction temperature is at 200°C. The low reaction temperature is unbeneficial to the formation of the core and the decrease in surface defects [48], while the excessively high temperature would cause serious carbonization of prepared CDs and destroy the surface fluorophores of prepared CDs (the CD solution prepared at 210°C exhibits a darker color), leading to a decrease in fluorescence intensity.

With other parameters fixed (1.0 g DL-malic acid and 0.4 mL EDA, 200°C), the impact of reaction time (2 h-7 h) upon the fluorescence intensity of the products was also investigated. As shown in Figure 2(b), with the increase in reaction time from 2 h to 4 h, the fluorescence intensity of prepared CDs enhances and then stays stable (4 h-5 h). However, when the reaction time surpasses 5 h, the color of the product turns dark with an obvious decrease in PL intensity. The optimal reaction time is thus set at 4 h. Under high temperature, DL-malic acid and EDA first undergo dehydration condensation reactions and form polymers, and the polymer then is carbonized into the carbon core [49]. The long reaction time is beneficial to the decomposition of EDA and thus increased the doping ratio of the N element in the carbon core. Through the above experiments, the optimal reaction parameters are 1.0 g DL-malic acid and 0.4 mL EDA which react at 200°C for 4 h. With rhodamine 6G as the reference, the QY of CDs prepared at optimal conditions is 38.2%.

3.1.3. Characterization of CDs. As shown in Figure 3, there exists an obvious absorption peak at 324 nm in CDs' UV-Vis absorption spectra, which originates from the $n-\pi^*$ transition of the surface group. The prepared CDs emit a bright green fluorescence under the illumination of UV light (365 nm).

The element composition of prepared CDs set a great impact upon the fluorescence properties. IR and EDS were used to analyze the surface groups and element composition of prepared CDs. As shown in Figure 4(a), the absorption peak at 3300 cm^{-1} originates from the stretching vibration of C-OH and N-H, the peaks at 3061 cm^{-1} and 2936 cm^{-1} from the stretching vibration of C-H, the peak at 1650 cm^{-1} from the stretching vibration of C=O, the peak at 1565 cm^{-1} from the bending vibration of N-H, the peak at 1390 cm^{-1} from the stretching vibration of C-N, and the peaks at 1182 cm^{-1} and 1086 cm^{-1} from the bending vibration of C-H. These surface groups are similar to those of CDs prepared by a microwave route [13]. The –COOH and -NH_2

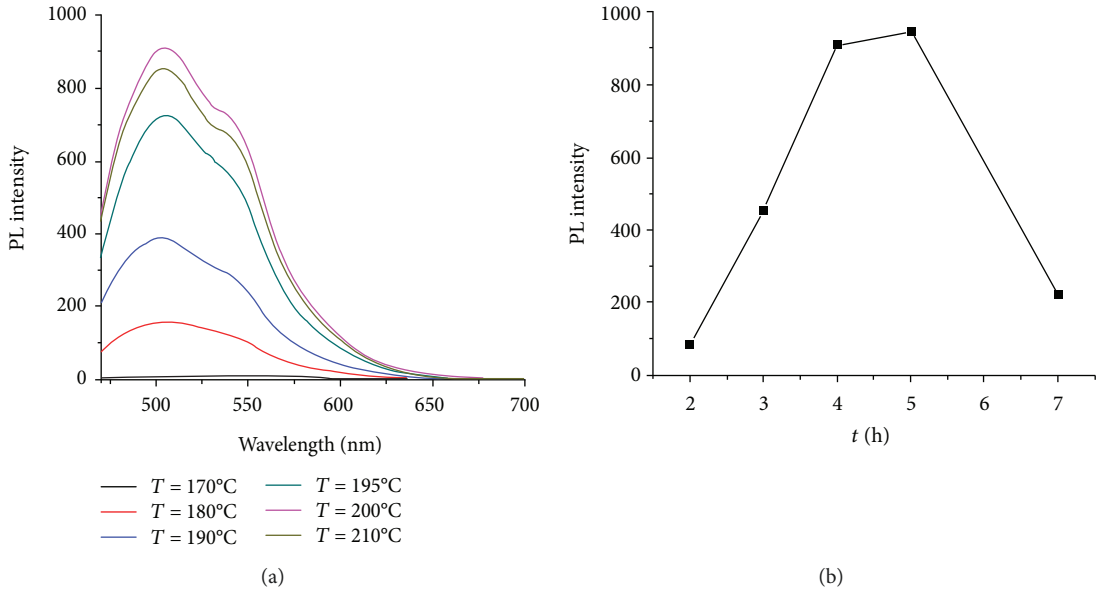

Figure 2: Effect of (a) reaction temperatures and (b) reaction times on the PL spectra of CDs (λ_{ex} = 460 nm, λ_{em} = 500 nm).

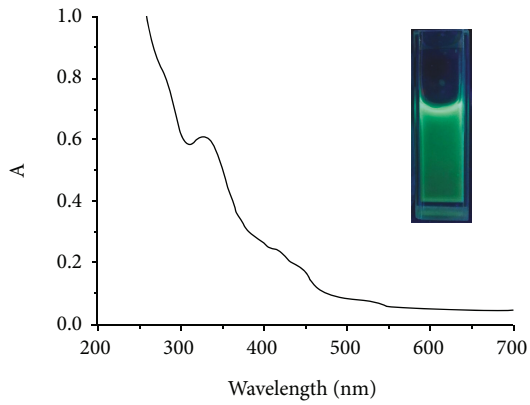

Figure 3: UV-Vis absorption spectrum of CDs. Inset: photographs of CDs under UV light at 365 nm.

groups show excellent water solubility of CDs, beneficial to their application in biochemical detections.

As shown in Figure 4(b), CDs are mainly composed of three elements, C, N, and O, with their ratios at 88.4%, 10.9%, and 0.7% wt, respectively. The N content of CDs prepared by the hydrothermal route is higher than that of CDs prepared by the microwave route (4.07%) [13]. The low temperature during the synthesis of CDs prepared by the microwave route (800w, 7 min) is not beneficial to the decomposition of EDA and the doping of the N element, while the N element has a positive effect on QYs [45]. This may be the reason why the QY of hydrothermal synthesis of CDs is higher than that of microwave synthesis of CDs. The crystallinity state of CDs is judged from the XRD pattern (Figure S1), which displays a clear broad peak at around 23°, demonstrating an amorphous property [50] of the CDs prepared in our case. The HRTEM image of the CDs is shown in Figure S8. The CD particles are spherical and monodispersed. The particle size distribution is 2.73-4.27 nm, and the average particle size is about 3.51 nm.

XPS measurements were performed to identify the detail of the chemical bond compositions. As shown in Figure 5(a), the full XPS spectra display three typical peaks at 285, 400, and 531 eV for C1s, N1s, and O1s, respectively, indicating that the CDs consisted of C, N, and O elements. In the high-resolution XPS spectra (Figure 5(b)), the C1s band can be deconvoluted into three binding energy peaks at 284.6, 286.1, and 288.3 eV, which could be assigned to C-C/C=C, C-O, and C=O, respectively. The N1s spectra Figure 5(c) display two peaks at 399.8 and 399.5 eV, attributed to N-C and –NH groups, respectively. O1s (Figure 5(d)) exhibits two main bands at 531.9 eV and 530.6 eV, confirming C-OH/C-O-C [51] and C=O [52], respectively. All these results of XPS are in agreement with FTIR results.

Because of the long-wavelength emission and strong luminescence of CDs, CDs are used to enhance the visualization of latent fingerprints. Figure 6(a) shows the PL images of sebaceous fingerprints (sebum-rich) developed by CDs. Sebaceous fingerprints were obtained by volunteers gently rubbing their fingertips over the forehead or nose, followed by stamping them on the aluminum foil with minimal pressure. The foil was immersed in the solution of the CDs under stirring for 30 min, followed by washing with water and drying under air. Photographs were taken under 365 nm UV light using a multimode microplate reader. The luminescence of fingerprints is sufficiently strong such that it can even overcome the reflection light from the blue background luminescence from the aluminum foil. Such results confirm our hypothesis that the large amount of -COOH on the CD's surface can promote the electrostatic interaction between CDs and fatty residues of latent fingerprints, enhancing the visualization of latent fingerprints. The excellent PL properties of CDs have ensured their potential application as fluorescence ink. The aqueous solution of CDs was directly injected into a pen without any chemical modification. Moreover, it was

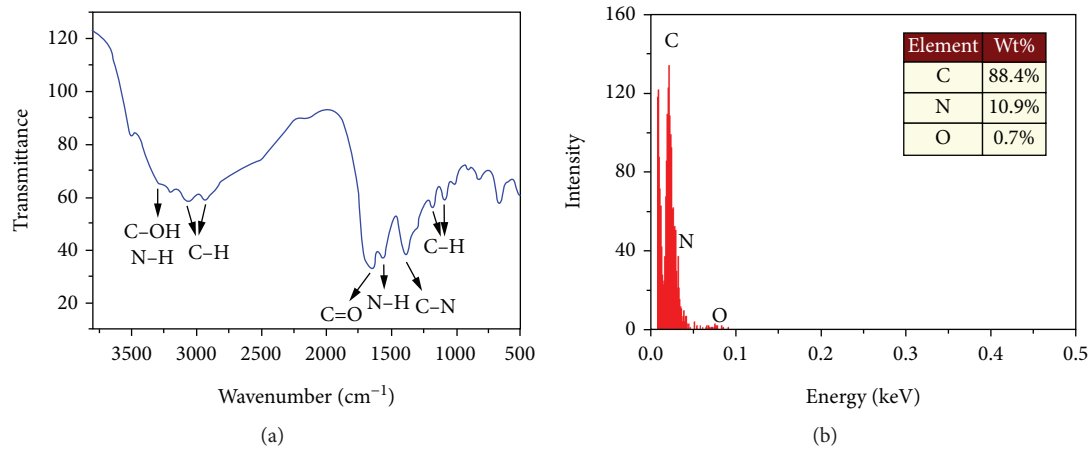

FIGURE 4: (a) IR spectrum and (b) EDS pattern of CDs. Table in the inset presents the elemental ratios.

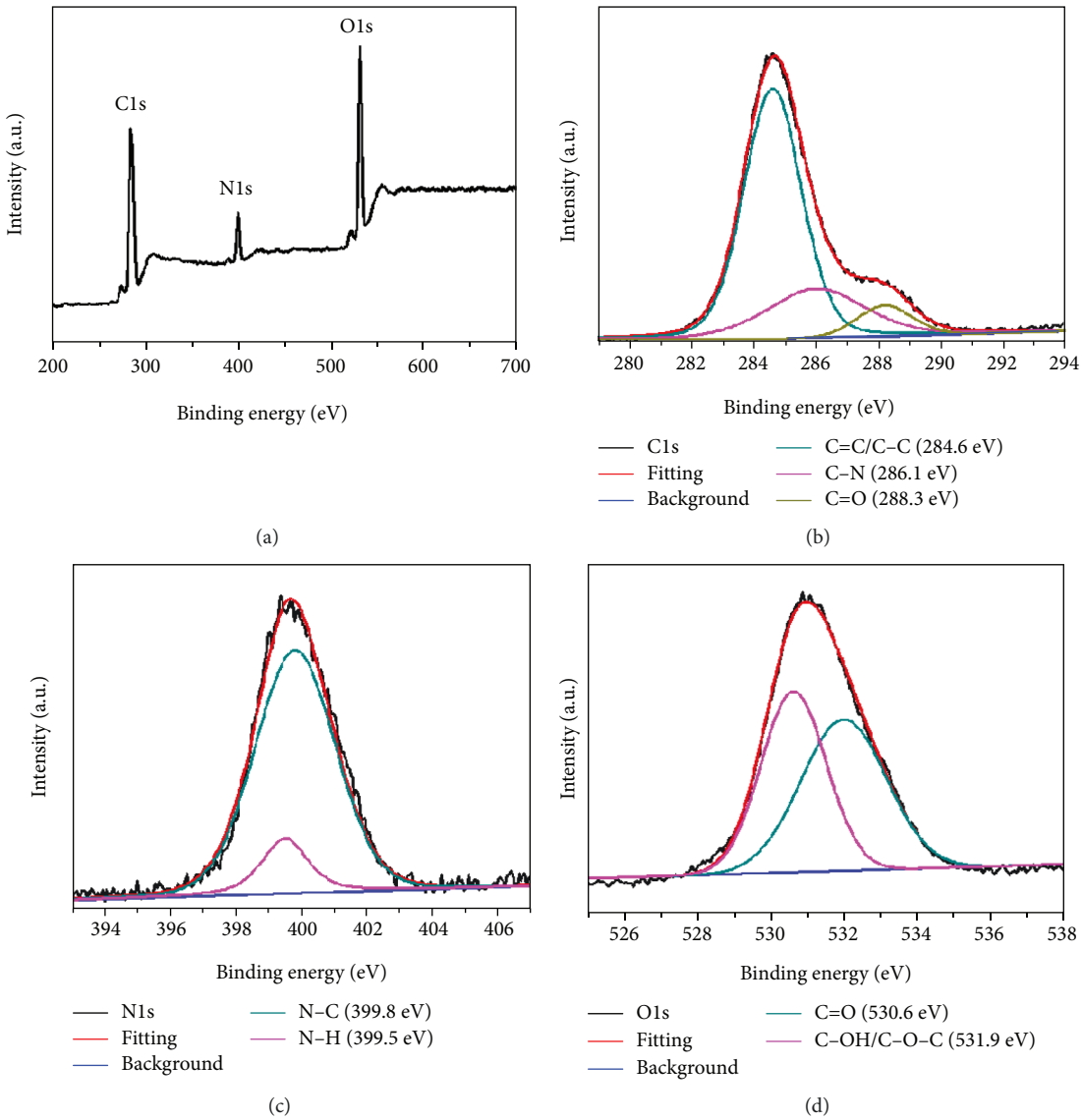

FIGURE 5: (a) XPS full-survey, high-resolution XPS of (b) C 1s, N1s (c), and (c) O 1s spectra for CDs.

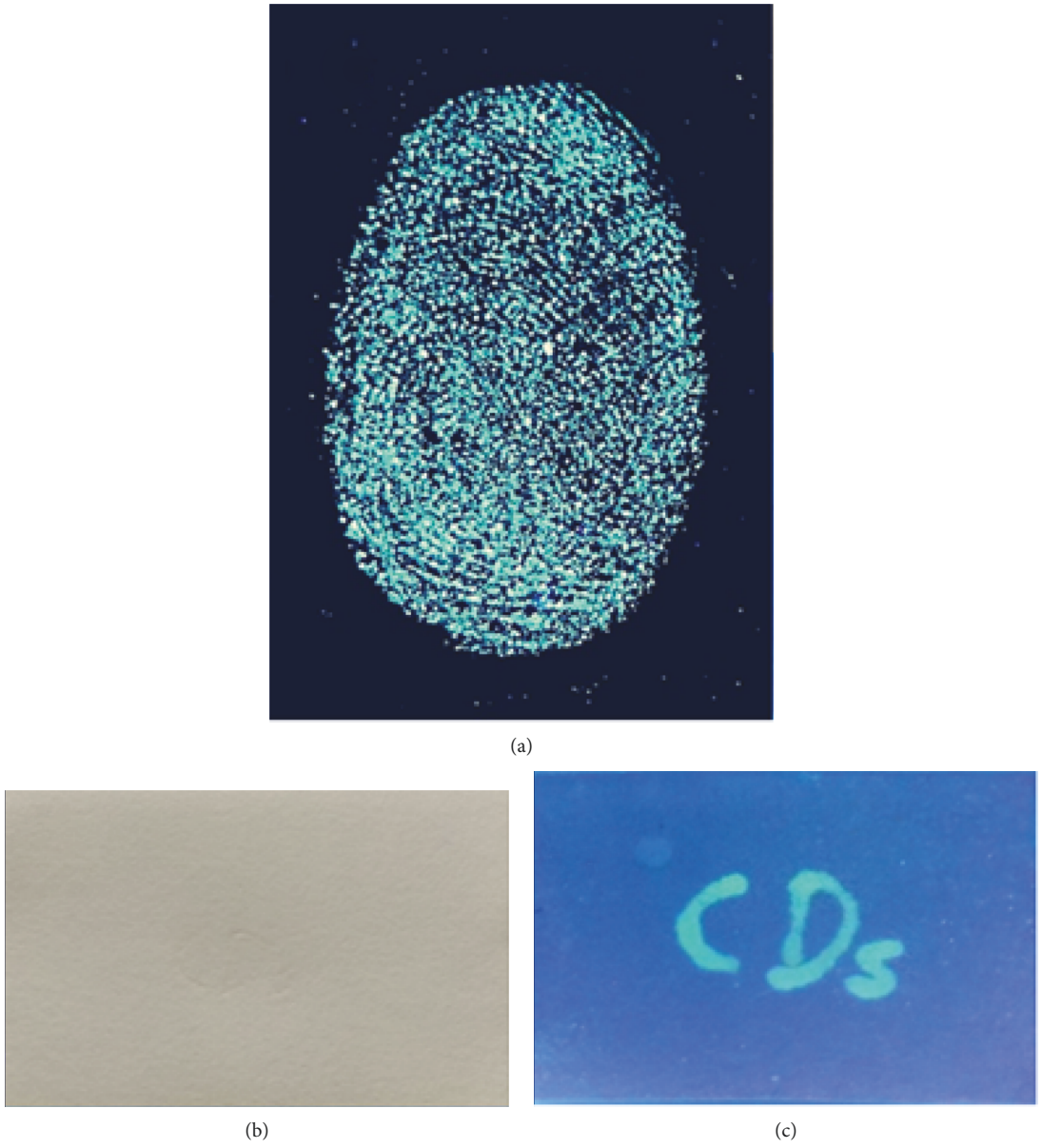

(a)

(b) (c)

Figure 6: Green-emitting CDs formed a fingerprint on aluminum foil under UV lamp irradiation (a); photographs of PL characters written with CDs on filter paper captured under room light (b) and UV light (c).

readily flowing while writing without any leakage and coagulation within the pen. As shown in Figures 6(b) and 6(c), the handwriting on a filter paper was colorless under ambient light but showed bright green fluorescence under UV light at a wavelength of 365 nm.

3.2. The Detection of Fe^{2+} Based on IFE

3.2.1. The Detection of Fe^{2+} and Its Mechanism. The prepared CDs ($\lambda_{em} = 488$ nm) can serve as the fluorescence probe of the detection of Fe^{2+} in the aqueous phase ($\lambda_{ex} = 430$ nm, the concentration of CDs is 0.5 mg/mL). Since the pH stability and salt resistance of CDs would interfere the selectivity and sensitivity of the detection system, the anti-interference ability was thus investigated. At the same time, as shown in Figure S2, the separate addition of 2×10^{-5} mol/L Hg^{2+}, Pb^{2+}, Co^{3+}, Ag^{+}, Ca^{2+}, Zn^{2+}, Mn^{2+}, Fe^{3+}, and Fe^{2+} into the CD solution set almost no impact upon the fluorescence of CDs. In order to achieve the detection of Fe^{2+}, IFE is thus applied in the detection.

In order to choose suitable complexing agents, reagents that are easy to complex with Fe^{2+} were tested, such as HAc, PAA, CA, GI, urea, EDTA-2Na, and o-phen. Figure S3 exhibits that the existence of complexing agents (1.8×10^{-4} mol/L) does not cause obvious fluorescence intensity decrease after the addition of 2×10^{-5} mol/L Fe^{2+} into the CD solution, except that of o-phen. This occurs because the orange complex formed by Fe^{2+} and o-phen have an obvious absorption peak at 512 nm, while the PL spectrum of CDs exhibit an absorption peak at 488 nm (Figure 7). The overlapping of the UV absorption peak of the Fe^{2+}-o-phen complex and the fluorescence emission

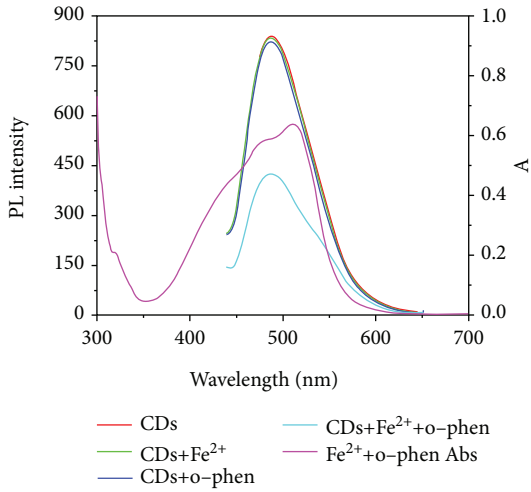

Figure 7: PL spectra of CDs, CDs and Fe^{2+}, CDs and o-phen, CDs and Fe^{2+}, and o-phen ($\lambda_{ex} = 430$ nm), UV-Vis absorption spectra of Fe^{2+} and o-phen complexes.

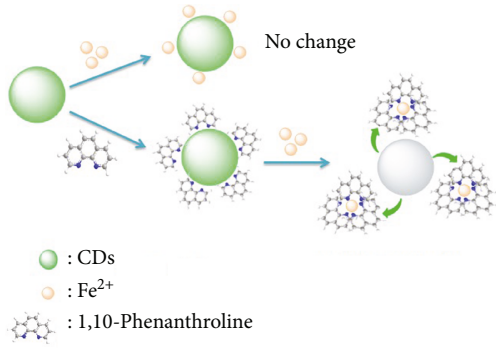

Figure 8: Schematic illustration for the detection of Fe^{2+} based on IFE.

peak of CDs occurred. Based on the IFE process, the complex can effectively quench the fluorescence of CDs [53].

The mechanism for detecting Fe^{2+} based on IFE is shown in Figure 8. There is no effect on the fluorescence of CDs when only Fe^{2+} or o-phen is present in the system. The fluorescence of CDs was quenched in the presence of $Fe^{2+}$and o-phen. In this system, Fe^{2+} and o-phen form an orange complex with a distinct absorption peak at 512 nm (as shown in Figure 7), which overlaps with the fluorescence emission peak of CD. Therefore, the complex formed by Fe^{2+} and o-phen can absorb the fluorescence emitted by CDs, thereby effectively quenching the fluorescence of CDs.

Meanwhile, the impacts of other metal ions that can easily complex with o-phen such as Co^{2+}, Mn^{2+}, Cd^{2+}, Cu^{2+}, Zn^{2+}, Fe^{3+}, and Ag^{+} (2×10^{-5} mol/L) upon the fluorescence intensity of CDs were also investigated (Figure S4); the effects of complexes formed by other metal ions and o-phen on the fluorescence intensity of CDs are negligible. Therefore, our system of o-phen-CDs can specifically detect the existence of Fe^{2+} and can also effectively distinguish Fe^{2+} from Fe^{3+}, which cannot be realized by some methods (such as atomic absorption spectrometry).

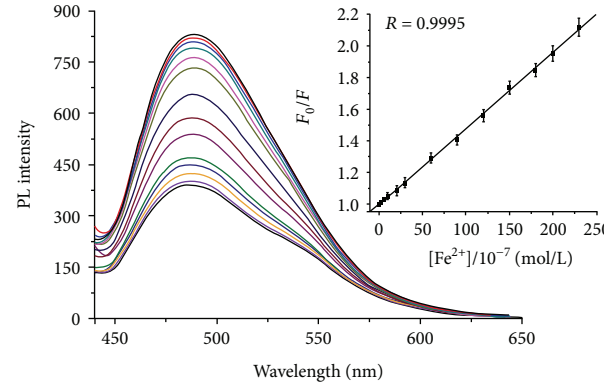

Figure 9: PL spectra of CDs in the presence of increasing amounts of Fe^{2+} ($[Fe^{2+}] = 2$, 5, 10, 20, 30, 60, 90, 120, 150, 180, 200, and 230×10^{-7} mol/L). Inset: the Stern-Volmer plot of CDs quenched by Fe^{2+}. Every data point was the mean of three measurements. The error bars are the standard deviation ($\lambda_{ex} = 430$ nm, $\lambda_{em} = 488$ nm).

3.2.2. The Detection of Fe^{2+}. The effects of reaction time, optimal pH value of the buffer, and concentration of o-phen were determined, and the results are shown in Figure S5-S7. Shown in Figure 9 are the PL spectra of CDs in the presence of various concentrations of Fe^{2+} in the Tris-HCl buffer (20 mmol/L, pH = 7). As shown from the standard curve of fluorescence intensity to Fe^{2+} concentration ($\lambda_{ex} = 430$ nm, inset of Figure 9), the fluorescence intensity of CDs decreases with the enhancement of Fe^{2+} concentration. The quenching can be expressed with the Stern-Volmer equation:

$$\frac{F_0}{F} = 1 + K_{sv}[c], \quad (1)$$

where F_0 and F are the fluorescence intensities of CDs before and after the addition of Fe^{2+}, K_{sv} is the quenching constant, and $[c]$ is the concentration of the detection target. The system exhibits good linearity in the range of 2.0×10^{-7} – 2.3×10^{-5} mol/L, $F_0/F = 0.99647 + 0.00481[c]$, $R = 0.9995$.

In order to verify the practical application value of this method, we applied it to the quantification of Fe^{2+} in commercial drug ferrous sulfate syrup. Ferrous sulfate syrup is an iron supplement. If it is not properly preserved, Fe^{2+} will be oxidized to Fe^{3+}, so it is necessary to detect the concentration of Fe^{2+}. We used a simple dilution method to dilute the ferrous sulfate syrup to a concentration of Fe^{2+} of 1.2×10^{-6} mol/L and calculate its detection concentration of 1.15×10^{-6} mol/L through the Stern-Volmer equation. Finally, we calculated a recovery of 95.8% and a relative standard deviation of 1.8% ($n = 3$).

4. Conclusion

This paper reports the simple preparation method of green-emissioned CDs through the hydrothermal route with DL-malic acid and EDA as the raw material, and the optical properties and structure of the prepared CDs have been further studied through UV-Vis absorption spectra, fluorescence spectra, FTIR, EDS, and XPS. The QYs of prepared

CDs reached 38.2% under optimal synthesis environment, and the CDs exhibit excellent pH stability and salt resistance, eligible for fingerprint development and fluorescence ink. Moreover, a new detection method with CDs as a fluorescence probe to realize the direct, effective, and specific detection of Fe^{2+} through IFE have been proposed, and the system is proven to be effective in the range of $2.0 \times 10^{-7} - 2.3 \times 10^{-5}$ mol/L with good interference immunity, setting a solid foundation for its future application in the detection of Fe^{2+} in cells and other biological systems.

Data Availability

The [DATA TYPE] data used to support the findings of this study are included within the supplementary information file(s).

Conflicts of Interest

The authors declare that they have no conflicts of interest.

Acknowledgments

This research was supported by the Natural Science Foundation of Hubei Province (2016CFB615), the Fundamental Research Funds for the "Central Universities", South Central University for Nationalities (CZY15020, CZW15017), and the Academic Team of South Central University for Nationalities (XTZ15013).

Supplementary Materials

Figure S1: XRD pattern of CDs. Figure S2: effect of metal ions on the PL intensity of CDs. Figure S3: effect of different complexing agents on the detection system. Figure S4: different metal ions on the detection system interference. Figure S5: (a) effect of buffer pH on the PL intensity of CDs; (b) effect of the concentration of NaCl on the PL intensity of CDs. Figure S6: (a) effect of reaction time on the detection of Fe^{2+}; (b) effect of buffer pH on the detection of Fe^{2+}. Figure S7: effect of o-phen on the detection of Fe^{2+}. Figure S8: HRTEM image and the size distribution (inset) of CDs. *(Supplementary Materials)*

References

[1] Y. Wu, P. Wei, S. Pengpumkiat, E. A. Schumacher, and V. T. Remcho, "Development of a carbon dot (C-dot)-linked immunosorbent assay for the detection of human α-fetoprotein," *Analytical Chemistry*, vol. 87, no. 16, pp. 8510–8516, 2015.

[2] P. Shen and Y. Xia, "Synthesis-modification integration: one-step fabrication of boronic acid functionalized carbon dots for fluorescent blood sugar sensing," *Analytical Chemistry*, vol. 86, no. 11, pp. 5323–5329, 2014.

[3] W. Yang, H. Zhang, J. Lai et al., "Carbon dots with red-shifted photoluminescence by fluorine doping for optical bio-imaging," *Carbon*, vol. 128, pp. 78–85, 2018.

[4] M. Lan, S. Zhao, Z. Zhang et al., "Two-photon-excited near-infrared emissive carbon dots as multifunctional agents for fluorescence imaging and photothermal therapy," *Nano Research*, vol. 10, no. 9, pp. 3113–3123, 2017.

[5] S. L. D'souza, S. S. Chettiar, J. R. Koduru, and S. K. Kailasa, "Synthesis of fluorescent carbon dots using *Daucus carota* subsp. *sativus* roots for mitomycin drug delivery," *Optik*, vol. 158, pp. 893–900, 2018.

[6] L. Yang, Z. Wang, J. Wang et al., "Doxorubicin conjugated functionalizable carbon dots for nucleus targeted delivery and enhanced therapeutic efficacy," *Nanoscale*, vol. 8, no. 12, pp. 6801–6809, 2016.

[7] F. Wang, P. Chen, Y. Feng et al., "Facile synthesis of N-doped carbon dots/g-C_3N_4 photocatalyst with enhanced visible-light photocatalytic activity for the degradation of indomethacin," *Applied Catalysis B: Environmental*, vol. 207, pp. 103–113, 2017.

[8] C. Sun, Y. Zhang, K. Sun et al., "Combination of carbon dot and polymer dot phosphors for white light-emitting diodes," *Nanoscale*, vol. 7, no. 28, pp. 12045–12050, 2015.

[9] H. Nie, M. Li, Q. Li et al., "Carbon dots with continuously tunable full-color emission and their application in ratiometric pH sensing," *Chemistry of Materials*, vol. 26, no. 10, pp. 3104–3112, 2014.

[10] J. Hou, W. Wang, T. Zhou, B. Wang, H. Li, and L. Ding, "Synthesis and formation mechanistic investigation of nitrogen-doped carbon dots with high quantum yields and yellowish-green fluorescence," *Nanoscale*, vol. 8, no. 21, pp. 11185–11193, 2016.

[11] A. Sciortino, N. Mauro, G. Buscarino et al., "β-C_3N_4 nanocrystals: carbon dots with extraordinary morphological, structural, and optical homogeneity," *Chemistry of Materials*, vol. 30, no. 5, pp. 1695–1700, 2018.

[12] C. Wei, J. Li, X. Xiao, T. Yue, and D. Zhao, "The one-step preparation of green-emission carbon dots based on the deactivator-reducing reagent synergistic effect and the study on their luminescence mechanism," *RSC Advances*, vol. 8, no. 36, pp. 20016–20024, 2018.

[13] S. Pang, Y. Zhang, C. Wu, and S. Feng, "Fluorescent carbon dots sensor for highly sensitive detection of guanine," *Sensors and Actuators B: Chemical*, vol. 222, pp. 857–863, 2016.

[14] Y.-Y. Ding, X.-J. Gong, Y. Liu et al., "Facile preparation of bright orange fluorescent carbon dots and the constructed biosensing platform for the detection of pH in living cells," *Talanta*, vol. 189, pp. 8–15, 2018.

[15] J. Zheng, J. Wang, Y. Wang, Y. Yang, X. Liu, and B. Xu, "Facile and rapid synthesis of yellow-emission carbon dots for white light-emitting diodes," *Journal of Electronic Materials*, vol. 47, no. 12, pp. 7497–7504, 2018.

[16] H. Li, X. Yan, S. Qiao, G. Lu, and X. Su, "Yellow-emissive carbon dot-based optical sensing platforms: cell imaging and analytical applications for biocatalytic reactions," *ACS Applied Materials & Interfaces*, vol. 10, no. 9, pp. 7737–7744, 2018.

[17] Z. Han, K. Wang, F. du, Z. Yin, Z. Xie, and S. Zhou, "High efficiency red emission carbon dots based on phenylene diisocyanate for trichromatic white and red LEDs," *Journal of Materials Chemistry C*, vol. 6, no. 36, pp. 9631–9635, 2018.

[18] H. Ding, Y. Ji, J. S. Wei, Q. Y. Gao, Z. Y. Zhou, and H. M. Xiong, "Facile synthesis of red-emitting carbon dots from pulp-free lemon juice for bioimaging," *Journal of Materials Chemistry B*, vol. 5, no. 26, pp. 5272–5277, 2017.

[19] C. Wang, K. Jiang, Q. Wu, J. Wu, and C. Zhang, "Green synthesis of red-emitting carbon nanodots as a novel "turn-on"

nanothermometer in living cells," *Chemistry - A European Journal*, vol. 22, no. 41, pp. 14475–14479, 2016.

[20] K. Jiang, S. Sun, L. Zhang et al., "Red, green, and blue luminescence by carbon dots: full-color emission tuning and multicolor cellular imaging," *Angewandte Chemie International Edition*, vol. 54, no. 18, pp. 5360–5363, 2015.

[21] X. Miao, D. Qu, D. Yang et al., "Synthesis of carbon dots with multiple color emission by controlled graphitization and surface functionalization," *Advanced Materials*, vol. 30, no. 1, 2018.

[22] Z. Wang, F. Yuan, X. Li et al., "53% efficient red emissive carbon quantum dots for high color rendering and stable warm white-light-emitting diodes," *Advanced Materials*, vol. 29, no. 37, article 1702910, 2017.

[23] F. Yuan, Z. Wang, X. Li et al., "Bright multicolor bandgap fluorescent carbon quantum dots for electroluminescent light-emitting diodes," *Advanced Materials*, vol. 29, no. 3, 2017.

[24] Y. Liu, N. Xiao, N. Gong et al., "One-step microwave-assisted polyol synthesis of green luminescent carbon dots as optical nanoprobes," *Carbon*, vol. 68, pp. 258–264, 2014.

[25] F. Li, T. Li, C. Sun, J. Xia, Y. Jiao, and H. Xu, "Selenium-doped carbon quantum dots for free-radical scavenging," *Angewandte Chemie*, vol. 129, no. 33, pp. 10042–10046, 2017.

[26] H. Ding, J. S. Wei, P. Zhang, Z. Y. Zhou, Q. Y. Gao, and H. M. Xiong, "Solvent-controlled synthesis of highly luminescent carbon dots with a wide color gamut and narrowed emission peak widths," *Small*, vol. 14, no. 22, 2018.

[27] D. Chen, et al.H. Gao, X. Chen, G. Fang, S. Yuan, and Y. Yuan, "Excitation-independent dual-color carbon dots: surface-state controlling and solid-state lighting," *ACS Photonics*, vol. 4, no. 9, pp. 2352–2358, 2017.

[28] Y.-J. Kim, H.-S. Jung, J. Lim, S.-J. Ryu, and J.-K. Lee, "Rapid imaging of latent fingerprints using biocompatible fluorescent silica nanoparticles," *Langmuir*, vol. 32, no. 32, pp. 8077–8083, 2016.

[29] S. Paul, K. Gayen, N. Nandi, and A. Banerjee, "Carbon nanodot-induced gelation of a histidine-based amphiphile: application as a fluorescent ink, and modulation of gel stiffness," *Chemical Communications*, vol. 54, no. 34, pp. 4341–4344, 2018.

[30] S. Lin, Y. Cheng, C. Lin, J. Fang, W. Xiang, and X. Liang, "Carbon nanodots with intense emission from green to red and their multifunctional applications," *Journal of Alloys and Compounds*, vol. 742, pp. 212–219, 2018.

[31] J. Zhu, S. Sun, K. Jiang, Y. Wang, W. Liu, and H. Lin, "A highly sensitive and selective fluorimetric probe for intracellular peroxynitrite based on photoinduced electron transfer from ferrocene to carbon dots," *Biosensors and Bioelectronics*, vol. 97, pp. 150–156, 2017.

[32] C. Liu, B. Tang, S. Zhang et al., "Photoinduced Electron transfer mediated by coordination between carboxyl on carbon nanodots and Cu^{2+} quenching photoluminescence," *The Journal of Physical Chemistry C*, vol. 122, no. 6, pp. 3662–3668, 2018.

[33] L. Ding, H. Yang, S. Ge, and J. Yu, "Fluorescent carbon dots nanosensor for label-free determination of vitamin B_{12} based on inner filter effect," *Spectrochimica Acta Part A: Molecular and Biomolecular Spectroscopy*, vol. 193, pp. 305–309, 2018.

[34] M. Zheng, Z. Xie, D. Qu et al., "On–off–on fluorescent carbon dot nanosensor for recognition of chromium (VI) and ascorbic acid based on the inner filter effect," *ACS Applied Materials & Interfaces*, vol. 5, no. 24, pp. 13242–13247, 2013.

[35] J. M. Jung, S. Y. Lee, and C. Kim, "A novel colorimetric chemosensor for multiple target metal ions Fe^{2+}, Co^{2+}, and Cu^{2+} in a near-perfect aqueous solution: experimental and theoretical studies," *Sensors and Actuators B: Chemical*, vol. 251, pp. 291–301, 2017.

[36] M. Mergelsberg, M. Willistein, H. Meyer et al., "Phthaloyl-coenzyme A decarboxylase from *Thauera chlorobenzoica*: the prenylated flavin-, K^{+}- and Fe^{2+}-dependent key enzyme of anaerobic phthalate degradation," *Environmental Microbiology*, vol. 19, no. 9, pp. 3734–3744, 2017.

[37] W. Hassan, H. Noreen, S. Rehman et al., "Oxidative stress and antioxidant potential of one hundred medicinal plants," *Current Topics in Medicinal Chemistry*, vol. 17, no. 12, pp. 1336–1370, 2017.

[38] S. Toyokuni, "Role of iron in carcinogenesis: cancer as a ferrotoxic disease," *Cancer Science*, vol. 100, no. 1, pp. 9–16, 2009.

[39] A. Matta, "Iron accumulation and neurodegeneration in patients with Alzheimer's diseases: an integrative review study of the evidence," *Neurology*, vol. 6, pp. 267–272, 2017.

[40] M. Patel and P. B. McElroy, "Mitochondrial dysfunction in Parkinson's disease," in *Oxidative Stress and Redox Signalling in Parkinson's Disease*, pp. 61–96, The Royal Society of Chemistry, 2017.

[41] G. Gao, Y. W. Jiang, H. R. Jia, J. Yang, and F. G. Wu, "On-off-on fluorescent nanosensor for Fe^{3+} detection and cancer/normal cell differentiation via silicon-doped carbon quantum dots," *Carbon*, vol. 134, pp. 232–243, 2018.

[42] H. Wu, J. Jiang, X. Gu, and C. Tong, "Nitrogen and sulfur co-doped carbon quantum dots for highly selective and sensitive fluorescent detection of Fe(III) ions and L-cysteine," *Microchimica Acta*, vol. 184, no. 7, pp. 2291–2298, 2017.

[43] T. G. Jo, K. H. Bok, J. Han, M. H. Lim, and C. Kim, "Colorimetric detection of Fe^{3+} and Fe^{2+} and sequential fluorescent detection of Al^{3+} and pyrophosphate by an imidazole-based chemosensor in a near-perfect aqueous solution," *Dyes and Pigments*, vol. 139, pp. 136–147, 2017.

[44] M. Grabolle, M. Spieles, V. Lesnyak, N. Gaponik, A. Eychmüller, and U. Resch-Genger, "Determination of the fluorescence quantum yield of quantum dots: suitable procedures and achievable uncertainties," *Analytical Chemistry*, vol. 81, no. 15, pp. 6285–6294, 2009.

[45] Y. Zhou, A. Desserre, S. K. Sharma et al., "Gel-like carbon dots: characterization and their potential applications," *Chemphyschem*, vol. 18, no. 8, pp. 890–897, 2017.

[46] X. Zhai, P. Zhang, C. Liu et al., "Highly luminescent carbon nanodots by microwave-assisted pyrolysis," *Chemical Communications*, vol. 48, no. 64, pp. 7955–7957, 2012.

[47] Y. Y. Zhang, M. Wu, Y. Q. Wang, X. W. He, W. Y. Li, and X. Z. Feng, "A new hydrothermal refluxing route to strong fluorescent carbon dots and its application as fluorescent imaging agent," *Talanta*, vol. 117, pp. 196–202, 2013.

[48] M. J. Krysmann, A. Kelarakis, P. Dallas, and E. P. Giannelis, "Formation mechanism of carbogenic nanoparticles with dual photoluminescence emission," *Journal of the American Chemical Society*, vol. 134, no. 2, pp. 747–750, 2011.

[49] C. Han, R. Wang, K. Wang et al., "Highly fluorescent carbon dots as selective and sensitive "on-off-on" probes for iron(III) ion and apoferritin detection and imaging in living

cells," *Biosensors and Bioelectronics*, vol. 83, pp. 229–236, 2016.

[50] K. Bankoti, A. P. Rameshbabu, S. Datta, B. Das, A. Mitra, and S. Dhara, "Onion derived carbon nanodots for live cell imaging and accelerated skin wound healing," *Journal of Materials Chemistry B*, vol. 5, no. 32, pp. 6579–6592, 2017.

[51] N. Wang, Y. Wang, T. Guo, T. Yang, M. Chen, and J. Wang, "Green preparation of carbon dots with papaya as carbon source for effective fluorescent sensing of Iron (III) and *Escherichia coli*," *Biosensors and Bioelectronics*, vol. 85, pp. 68–75, 2016.

[52] F. Nawaz, L. Wang, L. F. Zhu, X. J. Meng, and F. S. Xiao, "Ascorbic acid assisted green route for synthesis of water dispersible carbon dots," *Chemical Research in Chinese Universities*, vol. 29, no. 3, pp. 401–403, 2013.

[53] S. Lu, G. Li, Z. Lv et al., "Facile and ultrasensitive fluorescence sensor platform for tumor invasive biomaker β-glucuronidase detection and inhibitor evaluation with carbon quantum dots based on inner-filter effect," *Biosensors and Bioelectronics*, vol. 85, pp. 358–362, 2016.